MDPI

Application of Fiber Optics for Completion Design Optimization: A Methodological Approach and Key Findings

Ebrahim Fathi [1,*]**, Fatemeh Belyadi** [2]**, Mohammad Faiq Adenan** [1] **and Christian Pacheco** [1]

1 Petroleum and Natural Gas Engineering Department, West Virginia University, Morgantown, WV 26505, USA; mha0003@mix.wvu.edu (M.F.A.); christianpac96@hotmail.com (C.P.)
2 Obsertelligence LLC., Aubrey, TX 76227, USA; fatemeh.belyadi@gmail.com
* Correspondence: ebfathi@mail.wvu.edu; Tel.: +1-3042932449

Abstract: This study investigates the application of fiber optic technology to optimize completion design in a hydraulic fracture stimulation for Marcellus Shale Reservoir. With a focus on improving cluster efficiencies and overcoming interstage communication challenges, the research utilizes real-time data from distributed acoustic (DAS), temperature (DTS), and strain (DSS) measurements. The methodology comprises a comprehensive analysis of completion and stimulation reports, fiber optics, microseismic data, and well logs. Conducted at the MSEEL well pads, MIP, and Boggess, and equipped with permanent and deployable fiber optic cables, this study emphasizes that engineered/geomechanical completion design leads to sustained cluster efficiency and stage production performance. Inefficient cluster efficiencies are primarily linked to fracture communication. Recommendations include employing a geomechanical completion design, avoiding non-uniform high natural fracture zones during hydraulic fracture stimulations, implementing short stage length, and using more 100 mesh sand. These insights, derived from correlations between fracture counts, distributed strain sensing (DSS), cluster efficiency, production logging, and production data, offer significant implications for optimizing completion design in unconventional reservoirs. The effective application of fiber optic technology, providing real-time DAS, DTS, and slow strain data, proves instrumental in addressing interstage communication challenges, contributing to improved reservoir performances and cost-effective operations in hydraulic fracture stimulations.

Keywords: enhance gas recovery; completion design optimization; interstage communication; fiber optic technology; cluster efficiencies; hydraulic fracture stimulation; Marcellus Shale; MSEEL

1. Introduction

Over the past few years, the oil and gas sector has witnessed transformative changes through the adoption of advanced technologies, especially regarding drilling wells horizontally and implementing hydraulic fracturing across multiple stages. These innovations have given rise to the concept of 'smart wells', where fiber optic sensors play a critical role in enabling high-resolution monitoring and surveillance. The term 'smart wells' refers to wells equipped with remotely operated devices that control the process and have data measurement capabilities in the completion string [1]. This paradigm shift has led to a new era of well management and operation, enhancing the industry's ability to gather real-time data for informed decision-making.

Fiber optic cables, characterized by minuscule glass or plastic filaments that transmit light beams, have emerged as a high-speed data transmission medium. The use of fiber optic sensors provides acoustic or temperature data that are distributed along the wellbore, contributing to what is known as distributed sensing. This distributed sensing involves a sophisticated process where a laser pulse is transmitted through optical cables, utilizing total internal reflection to transmit light waves while generating backscattering signals as a result of flaws in the cable. These backscattered signals are collected at the surface and

analyzed based on their frequency, correlating with different types of scattering, such as Rayleigh, Brillouin, and Raman, which are each associated with specific types of data like DAS, DSS, and DTS [2,3].

The deployment of fiber optic cables can be temporary inside the well tubing or permanently installed behind the well casing, each serving distinct purposes. Permanent installations are geared towards near-wellbore monitoring, focusing on DAS and DTS backscatter signals. However, wireline-deployed fiber optic cables are better suited for far-field monitoring, emphasizing DSS backscatter signals. This distinction is critical, especially considering the complex fracture networks created during hydraulic fracturing treatments, necessitating a careful interpretation procedure for practical industry use [4].

The integration of fiber optic technology is not a recent development; it traces back to the pioneering work of Enright in 1955 [5], who first proposed the concept of Distributed Acoustic Sensing (DAS). DAS detects sound vibrations along the length of the fiber optic cable. It works by measuring changes in scattered light, caused by sound disturbances, allowing optical fibers to act like continuous, high-detail, acoustic sensors. Subsequently, in 1962, Ramey [6] introduced Distributed Temperature Sensing (DTS) which turns the length of regular optical fibers into temperature sensors. By examining the scattered light within the fibers, DTS systems can identify temperature fluctuations along the fiber, offering continuous and detailed temperature information. Over the years, these technologies have evolved and have been utilized in various capacities within the oil and gas sector, including completion design optimization [7,8], production monitoring [9], reservoir depletion tracking [10], fracture monitoring [11], well interference studies [12], integrity monitoring during fracking [13], flow assurance during the completion stage [14], cleanup studies [15], the monitoring of subsequent stimulation fluids [16], and pipeline leak detection [17]. In addition to traditional numerical and lab studies on simulating hydraulic fractures [18], by studying how fractures spread [19] and how wellbores may be cleaned [20], we may understand how this technology can greatly enhance decision-making and the optimization of these processes. In 2012, Johanessen et al. [21], employed various techniques concerning Distributed Acoustic Sensing (DAS) measurements to analyze the flow along the wellbore. By analyzing the acoustic energy in the space frequency domain, they were able to calculate the speed of sound, providing valuable insights into the characteristics of the wellbore flow. This approach with DAS proves effective in detecting gas or water breakthroughs in oil production, as it enables the monitoring of spatial changes in the speed of sound. Additionally, Paleja et al. (2015) [22] demonstrated that DAS can reliably monitor the height of the liquid column in the annulus, particularly in gas–lift oil fields. Similarly, in 2012, Wang [23] introduced a novel approach using the least squares and linear inversion method. This method was applied to inner flow rates derived from Distributed Temperature Sensing (DTS) data. The outcome was a set of solutions describing the intricate relationship between flow, pressure, and temperature. Wang's work highlights the versatility of DTS data in providing comprehensive insights into the dynamic interplay of these critical parameters.

Field Case Study Demonstrating the Application of Fiber Optics

Given the widespread application of fiber optic technology, this study focuses on optimizing completion design in a hydraulic fracture stimulation, specifically in the Marcellus Shale reservoir. The Marcellus Shale Energy and Environmental Laboratory (MSEEL), started in partnership with Northeast Natural Energy LLC, universities, and the National Energy Technology Laboratory, serves as the research site. This facility, located in Monongalia County, West Virginia, operates wells in the central region of the Marcellus Shale, making it an ideal location for comprehensive research (Figure 1).
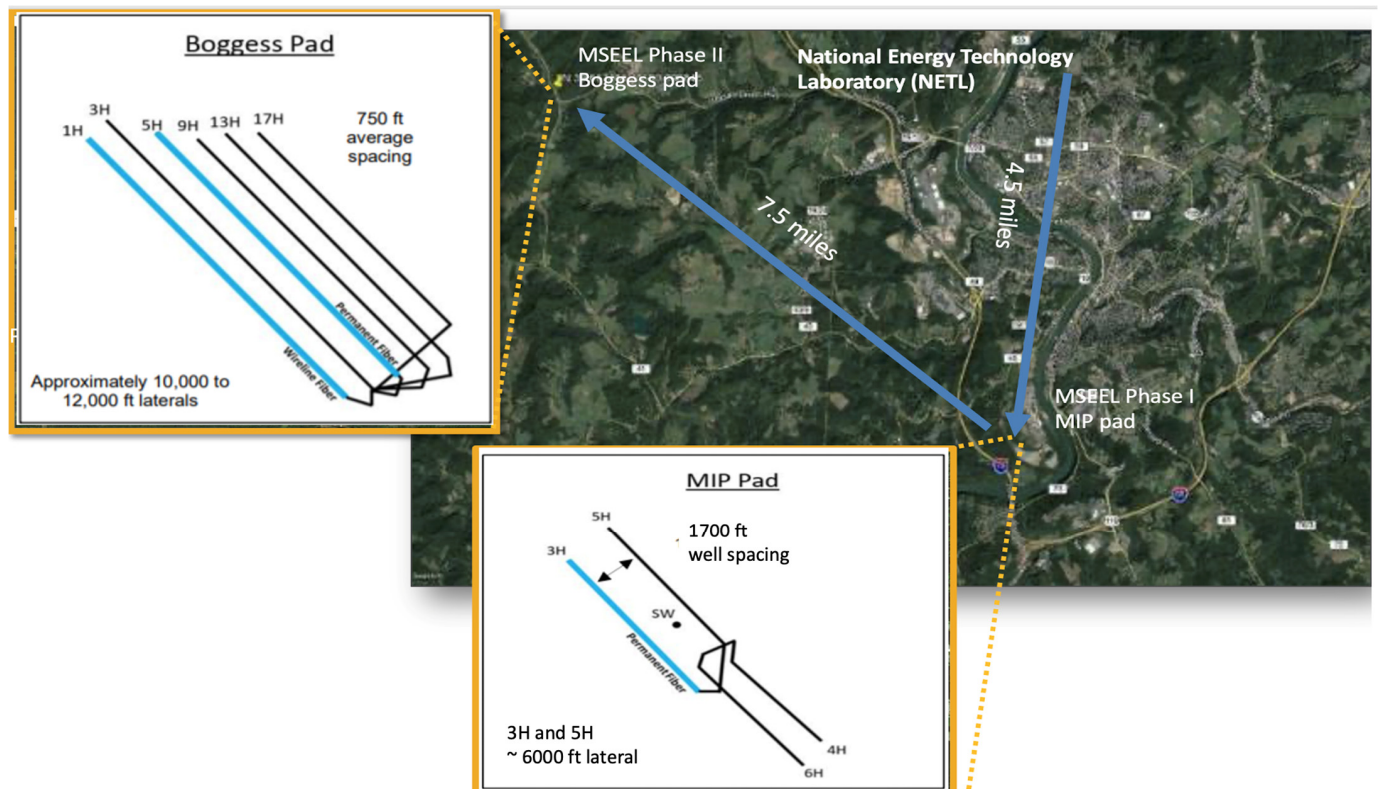
Figure 1. Location map showing the MIP and Boggess pads in the Marcellus Shale close to Morgantown, West Virginia (www.mseel.com).

Two primary well pads, MSEEL 1 and MSEEL 2, have been instrumental in testing and validating tools and processes that are both economical and offer the ability to immediately improve completion design efficiency and enhanced gas recovery from Marcellus Shale. MSEEL 1, situated in Morgantown, West Virginia, started operations in 2015. The drilling activities included MIP-3H and MIP-5H wells, along with the MIP-SW science and monitoring well. Data from previously drilled MIP-4H and MIP-6H wells in 2011 were also integrated into this site. The lateral MIP-3H underwent logging procedures and it was equipped with a permanent fiber-optic cable.

MSEEL 2, intended to enhance completion design, started its mission at the Boggess Pad, 12 km northwest of the MIP Pad, in fall 2015, as shown in Figure 1. The Boggess Pad includes six horizontal wells (Boggess 1H, 3H, 5H, 9H, 13H, and 17H) and a vertical science well. The full core and side walls are obtained from the science well, which is used for rock and fluid characterization. Formation micro imager log (FMI) and drilling acceleration data were obtained from all the wells in the Boggess pad, except Boggess 17H, which was used for predicting the number of natural fractures and their distribution using artificial intelligence and machine learning [24]. Permeant fiber optic cables installed in Boggess 5H were used to collect DAS, DTS, and DSS data during both the stimulation and production of the wells, whereas the deployable fiber optic used in Boggess 1H was only used during the stimulation period. All information and data used in this study are publicly available in website in Supplementary Materials.

The comprehensive dataset, including well logs, core analysis, and rock properties of the Marcellus Shale in both the MIP and Boggess pads (Tables 1 and 2), was used for the thorough investigation and hydrocarbon production optimization of Marcellus Shale.

Table 1. Top and bottom formations in both the MIP and Boggess pads.

	Well Log Analysis					
	Boggess			MIPH		
Formation	Formation Top (ft)	Formation Bottom (ft)	Thickness (ft)	Formation Top (ft)	Formation Bottom (ft)	Thickness (ft)
Geneseo Shale	7660	7690	30	7172	7190	18
Tully	7690	7770	80	7190	7285	95
Mahantango	7770	7880	110	7285	7456	171
Upper Marcellus	7880	7900	20	7456	7515	59
Cherry Valley	7900	7908	8	7515	7525	10
Lower Marcellus	7908	7975	67	7525	7555	30
Onondaga	7975	7995	20	7555	7800	245

Table 2. Marcellus shale rock properties in both the MIP and Boggess pads.

Pad	Boggess		MIPH	
Property	Value	Unit	Value	Units
Porosity	6.4	%	7	%
Permeability	400	nd	270	nd
Compressibility	5.5×10^{-6}	1/psi	5.0×10^{-5}	1/psi
TOC	8	%	5.48	%
Clay Volume (Upper Marcellus)	49.6	%	45	%
Clay Volume (Lower Marcellus)	20	%	22	%
Fracture Density	2.11	frac/ft	0.25	frac/ft
Young's Modulus	2.45×10^{6}	psi	2.2×10^{6}	psi
Poisson's Ratio	0.15		0.15	
Fracability Ratio	0.43		0.43	
Minimum Horizontal Stress Gradient	0.732–0.816	psi/ft	0.79–0.85	psi/ft
Mineralogy	Illite		Illite and Montmorillonite	

This study aims to address the current challenges associated with massive fracturing treatments and the creation of complex fracture networks. The main goal is to quantify the effectiveness of completion design techniques used in MSEEL projects and develop a practical use for fiber optic technology within the industry. Through an analysis of DAS and DTS data, along with microseismic data and advanced well logging, this study aims to optimize completion design, enhance cluster efficiencies, and tackle interstage communication challenges. These goals align with the broader industry objectives of achieving multiple robust and consistent hydraulic fracture networks along laterals [25] for an optimized stimulation design and maximized conductive reservoir volume [26]. This study represents a step forward in leveraging fiber optic technology to optimize completion designs for hydraulic fracture stimulation. The application of advanced sensing techniques and data analysis methods, combined with the rich dataset from MSEEL, contributes to a comprehensive understanding of reservoir behavior.

2. Methodology

In conventional completion design, three distinct techniques—geometric design, engineering or geomechanical design, and hybrid design (a blend of geometric and engineering

design)—are employed [27]. The MIP and Boggess pads have experienced varied completion design approaches, detailed in Table 3, encompassing well information such as completion design, true vertical depth (TVD), measured depth (MD), lateral length (LL), number of stages, and cumulative gas production.

Table 3. Boggess and MIP Well Pad Completion data.

Pad	Boggess						MIPH			
Well	1H	3H	5H	13H	9H	17H	MIP3H	MIP4H	MIP5H	MIP6H
Completion Design	Geomechanical Spacing			Geometrical Spacing			Hybrid Spacing	Geometrical Spacing		
True Vertical Depth, ft	8030	8030	8035	8020	8030	8020	7449	7571	7452	7499
Measured Depth, ft	20,872	21,075	20,226	20,298	19,835	19,026	13,869	11,213	14,454	9944
Lateral Length, ft	12,842	13,045	12,191	12,278	11,805	11,006	6420	3642	7002	2445
Number of Stages #	63	66	56	55	57	45	28	11	30	8
Production @ 6/22 (MMScf)	2350	2127	1794	1801	1816	1760	4451	2738	4076	1392

2.1. Completions Design of Boggess and MIP Pads

Within the Boggess pad, wells 9H, 13H, and 17H adopted a geometric design, featuring stages of 200 ft each, with an equal number of clusters. Notably, Boggess 5H employed a geomechanical design by a private consultant, incorporating geomechanical logs while disregarding imaged natural fractures. Conversely, engineer-designed wells 1H and 3H, by the MSEEL team, utilized a holistic approach, incorporating DTS and DAS data from well 5H, LWD image logs, drilling data, geomechanical logs, and the identification of natural fractures.

In the MIP pad, the geometric design was applied to three wells—MIP 4H, MIP 5H, and MIP 6H—whereas MIP 3H adopted a hybrid design. Figure 2 illustrates the details of the hybrid design implemented in MIP 3H. The well was strategically divided into five sections, denoted A through E, each employing distinct techniques.

Sections A and B encompass Stages 1 to 12, employing standard geometric spacing with evenly distributed stages. In Section A, a proppant mixture consisting of 35% 100 mesh and 65% 40/70 white sand was utilized. Section B introduced slight modifications to the stage length and the sand composition, using shorter stage lengths (SSL) and incorporating 75% 100 mesh sand and 25% 40/70 white sand.

Sections C to E cover Stages 13 to 28, which implemented "engineered" stage designs. This involved the utilization of a proprietary fluid system [28]. Engineered design factors include fracture closure stress, fracture counts, and gamma ray considerations. Clusters were strategically arranged to encounter similar stress zones. Proppant variations were significant, with stages 13, 14, 15, 17, and 19 containing 35% 100 mesh, whereas stage 16 employed 67% 100 mesh, and stage 18 included around 43% 100 mesh.

Section D incorporated an experimental approach from Schlumberger, employing a different frac fluid named Sapphire VF in stages 20 and 21. The use of this innovative fluid aimed to enhance proppant transportation, proppant retention permeability, fracture cleanup, and reduce treating pressure.

Section E covered the final stages (22–28), and a combination of an engineered design, sapphire fluid, and an accelerated pump schedule was used. Figure 2 details the MIP 3H engineering design with Track 1 illustrating the measured depth in the lateral section, Track 2 showcasing gamma ray data, and Track 3 revealing the transverse isotropic vertical (TIV) Minimum horizontal stress gradient that is crucial for geomechanical completion design.

This comprehensive approach optimizes the completion design by tailoring techniques to specific well sections, ensuring efficiency and effectiveness in the hydraulic fracture stimulation process.
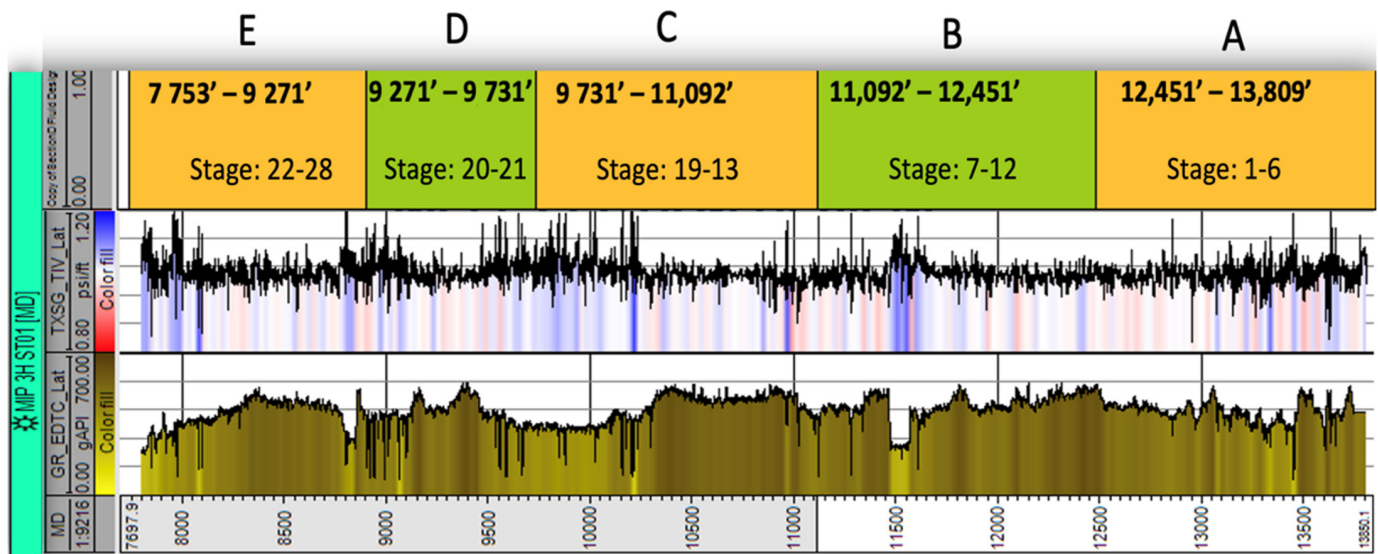

Figure 2. MIP 3H hybrid completion design with Track 1 illustrating measured depth in the lateral section, Track 2 showcasing gamma ray data, and Track 3 revealing the transverse isotropic vertical (TIV) Minimum horizontal stress gradient. (modified from [25]).

2.2. Fiber Optics Data Collected from Boggess and MIP Pads

The DAS and DTS data collected through permanent fiber optic cables (installed in MIP3H and Boggess 5H) and a deployable cable (in Boggess 1H), are critical for investigating cluster efficiency and gas production dynamics. DAS data revealed the breakthrough time, fracture propagation extent, and proppant placement quality. Continuous DTS data during flowback and production (up to three years post-initial production) quantified each stage's contribution to overall gas production. Findings from DTS and DAS data were compared with production logs (two years post-production start) to explore cluster and stage efficiency dynamics over time.

DSS data were leveraged to assess local strain changes during adjacent well stimulations, which shed light on well interference and Fracture-Driven Interactions (FDIs) between wells. DSS utilizes optical fibers as sensors to measure strain and deformation continuously. DSS data, being a subset of Distributed Acoustic Sensing (DAS), exclusively utilizes frequency signals below the 1 Hz range. DSS systems offer high-resolution monitoring for structural changes, which plays a crucial role in applications such as geotechnical monitoring. Natural fracture count logs, obtained from the Formation Microimager (FMI) log, as well as microseismic data, contributed to understanding well interference dynamics in both MIP and Boggess pads. A Stereonet diagram, shown in Figure 3, displays the natural fracture orientation obtained from FMI log interpretation. Figure 3 illustrates a comprehensive depiction of 6363 fracture counts with an N15° E orientation. After acquiring the natural fracture counts and distributions using a Formation Microimager (FMI) log, these values were utilized to discern Fracture-Driven Interactions (FDIs) through correlations with Distributed Strain Sensing (DSS) data collected from both permanent and deployable fiber optic cables.
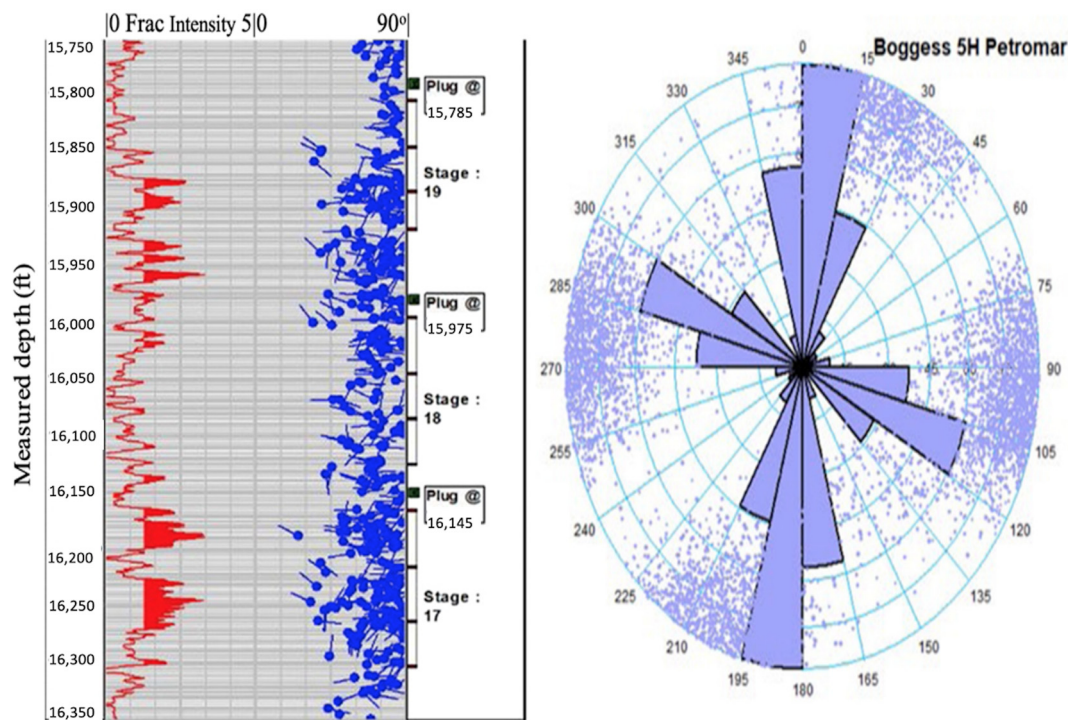
Figure 3. (**Left**): Fracture counts log of a portion of Boggess 5H [24], (**Right**): Stereonet diagram from fracture data obtained from Boggess 5H, showing 6363 fractures and the N15° E orientation [25].

For each stimulation stage in the Boggess pad, DSS data were collected from both permanent fiber optic cables installed in Boggess 5H, and deployable fiber optic cables in Boggess 1H, with a high resolution of 1 s for the whole measured depth of these two wells. Notably, data gathered for the Boggess 9H stimulation response were collected at Boggess 5H, data gathered for the Boggess 5H stimulation response were collected at Boggess 1H, and data gathered for the Boggess 9H stimulation response were collected at Boggess 1H.

The fiber optics data underwent pre-processing by assimilating second-by-second data obtained from each stage in a matrix format. Vertical sections of the well were discarded, and a column containing file timestamps was appended to the data frame. This information was then consolidated into a singular log per well. Subsequently, the logs were formatted into a pivot table, a memory-efficient structure, using a Python script. After employing Matplotlib, a Python-based open-source graphics package, heatmaps for each stage were generated. These heatmaps visualize interactions on the monitoring well with the fiber optic cable, displaying the time on the *y*-axis and depth on the *x*-axis, and the color intensity represents fiber optics data, such as Steady-State Thermo Reflectance (SSTR). SSTR leverages optical fibers to measure temperature changes in materials with high precision. By analyzing the reflection of heat-induced changes in the optical properties of the fiber, SSTR enables continuous and accurate temperature sensing in various applications.

To quantify the noise-to-data ratio, a visual step was undertaken to identify interactions. Using Tableau 2021.3, a data visualization software, we generated graphs depicting SSTR against timestep and depth, aligning with insights obtained from visual heatmaps (see Figure 4). Recognizing the correlation between time and depth, we developed a fracture counts log to facilitate the precise identification of FDI locations on the monitoring well, which were recorded using a 25 ft resolution (refer to Figure 5). We repeated this process for all the hydraulic fracturing stages, systematically documenting FDIs in a log that included stage details, SSTR values, measured depth locations of peak SSTR values, the depth associated with the maximum fracture counts, and the normalized SSSTR values via min–max normalization.
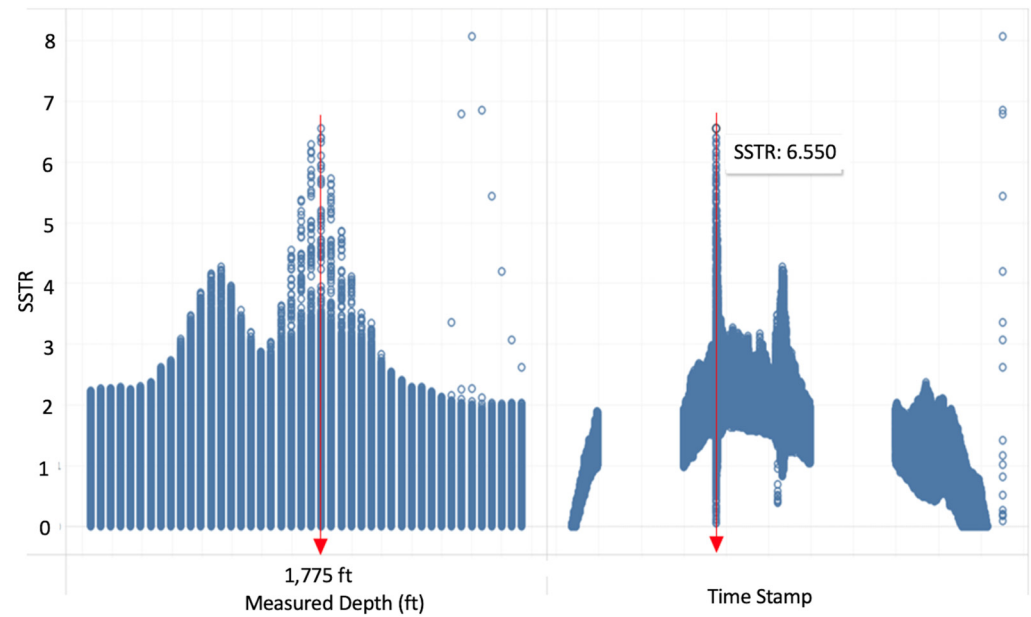
Figure 4. (**Left**): shows the depth correlated with the highest SSTR. (**Right**): the time associated with the highest SSTR monitoring well.
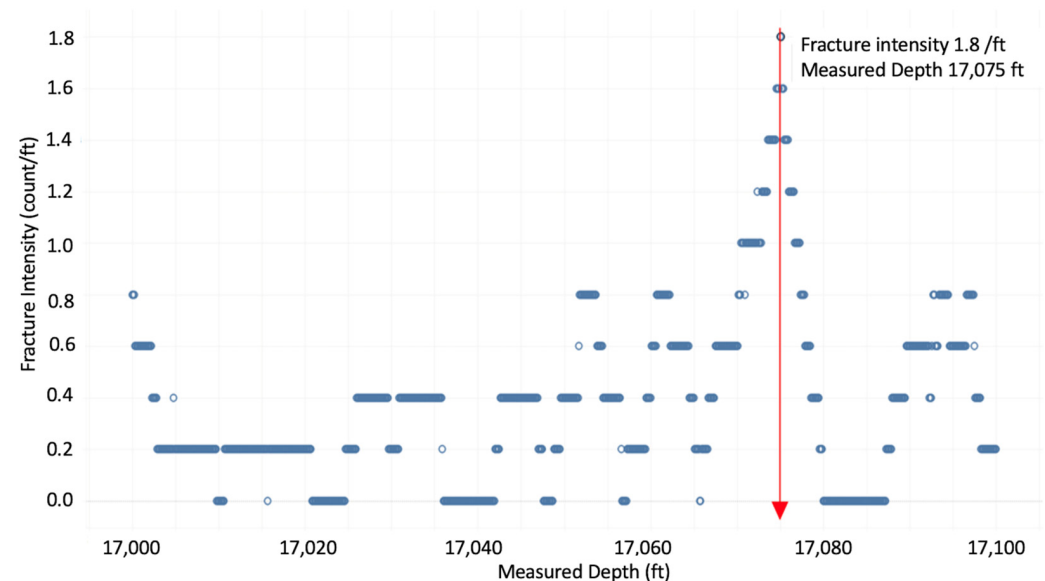

Figure 5. The depth correlated with the highest fracture counts from the monitoring well.

3. Results

3.1. MSEEL Phase I (MIP Pad)

In our initial investigation, we investigated the complexities of the MIP 3H well from the first phase of the MSEEL project, leveraging a substantial dataset of approximately 10 TB from fiber optic measurements. The extensive data, incorporating both DAS and DTS, facilitated an in-depth exploration into the impact of diverse completion design strategies on MIP 3H, as explained in Figure 2. This investigation yielded valuable insights into cluster efficiency, stress variations, production dynamics, among others, across multiple stages. The foundational step involved a comparative analysis of different completion designs, where their respective efficiencies were evaluated. The DAS data were instrumental in illustrating the energy distribution among clusters. In the initial stages (1 to 6) of the geometric stimulation treatment on MIP 3H, a non-uniform distribution of energy indicated a complex response, signifying non-uniform fracture propagation and lower

cluster efficiency. Challenges in achieving a balanced fracture network were highlighted, emphasizing the necessity for optimization strategies.

As we progressed to later stages (7 to 12), there were signs of improved responses which were influenced by treatment strategy adjustments. Despite these improvements, non-uniform fracture initiation persisted, impacting overall cluster efficiency. The use of shorter stage lengths (SSL) and a higher percentage of 100 mesh sand contributed to the observed enhancements, emphasizing the proppant selection's essential role in optimizing fracture propagation in Marcellus shale. Figure 6 illustrates stages from sections A and B, depicting depth on the *y*-axis, time on the *x*-axis, and the color bar representing Broadband energy strength. Stage 3 exhibited varying contributions to fracture development; the initial breakdown of clusters 3, 4, and 5 suggest potential fracture initiation, whereas clusters 1 and 2 became active later in the treatment, emphasizing the non-uniform response. Stage 6 further indicated non-uniform fracture initiation and progression due to the breakdowns of clusters 1, 2, and 3, with minimal energy in cluster 5, and almost no energy in cluster 4. Stages 8 and 10 demonstrated evolving (but still somewhat non-uniform) responses, prompting the need for further optimization.
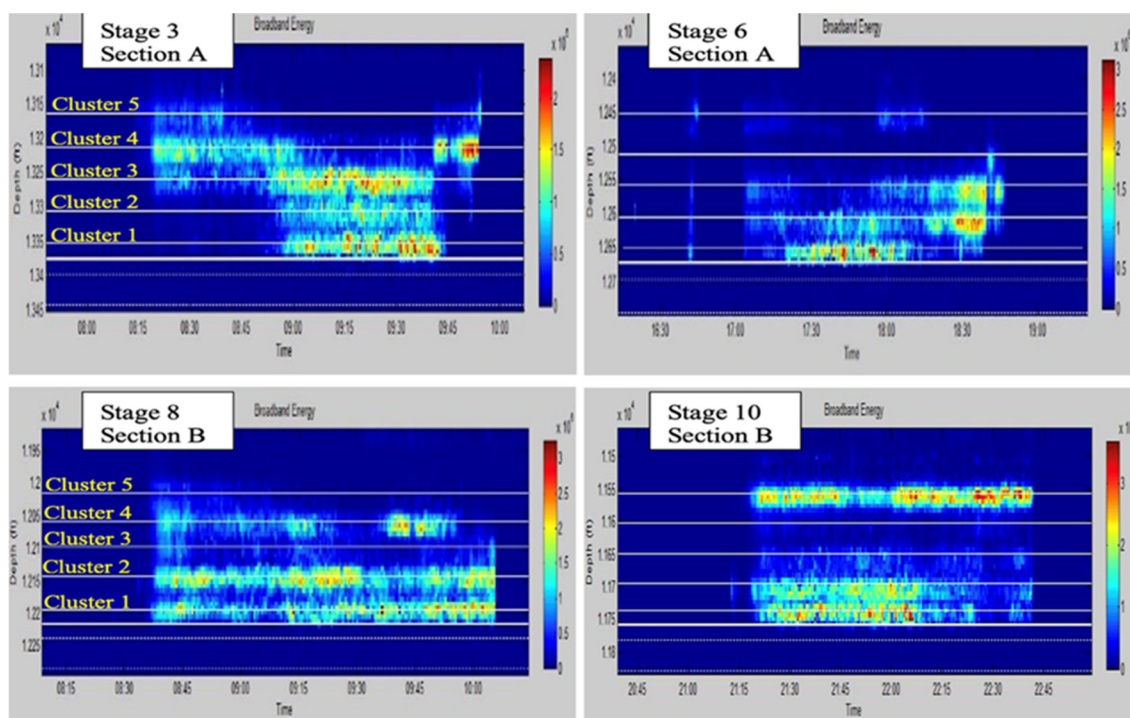

Figure 6. The Broadband energy received during the fracking of sections A and B of MIP3H, which were both created using a geometric completion design. The top shows stages 3 and 6 of Section A, with 35% 100 mesh, and the bottom shows stages 8 and 10 of Section B, with 75% 100 mesh (MIP3H completion www.mseel.com).

Section C employed an engineered or geomechanical completion design, guided by the Minimum Horizontal Stress Gradient log, in stages 13 to 19, and it showcased a markedly positive shift in the DAS analysis. The uniform and high-intensity energy distribution signaled enhanced fracture propagation and optimal sand placement, crucial for improved production efficiency. This success underscored the geomechanical approach's effectiveness in optimizing completion design and fostering a more favorable reservoir response.

The transition from earlier stages (1 to 12) to later stages (13 to 19) in Section C is reflective of a learning curve, with the latter stages demonstrating a refined and successful approach. Figure 7 illustrates DAS distribution in stages 14 and 18, revealing early breakthroughs in all clusters, and an effective Broadband energy distribution. Stage 18 implemented a shorter stage length (SSL), demonstrated improved energy distribution

between clusters, and aligned with previous studies that showcased SSL's positive impact on cumulative gas production from Marcellus Shale [29]. In Stage 18 of Section C, the length was reduced to 180 ft, compared with the design lengths of other stages, as follows: 238 ft for Stage 3, 245 ft for Stage 6, 222 ft for Stage 8, 227 ft for Stage 10, and 228 ft for Stage 14. Stage 18's reduced length, compared with previous stages, contributed to the enhanced efficiency observed in the distribution of energy and breakthroughs in all clusters.
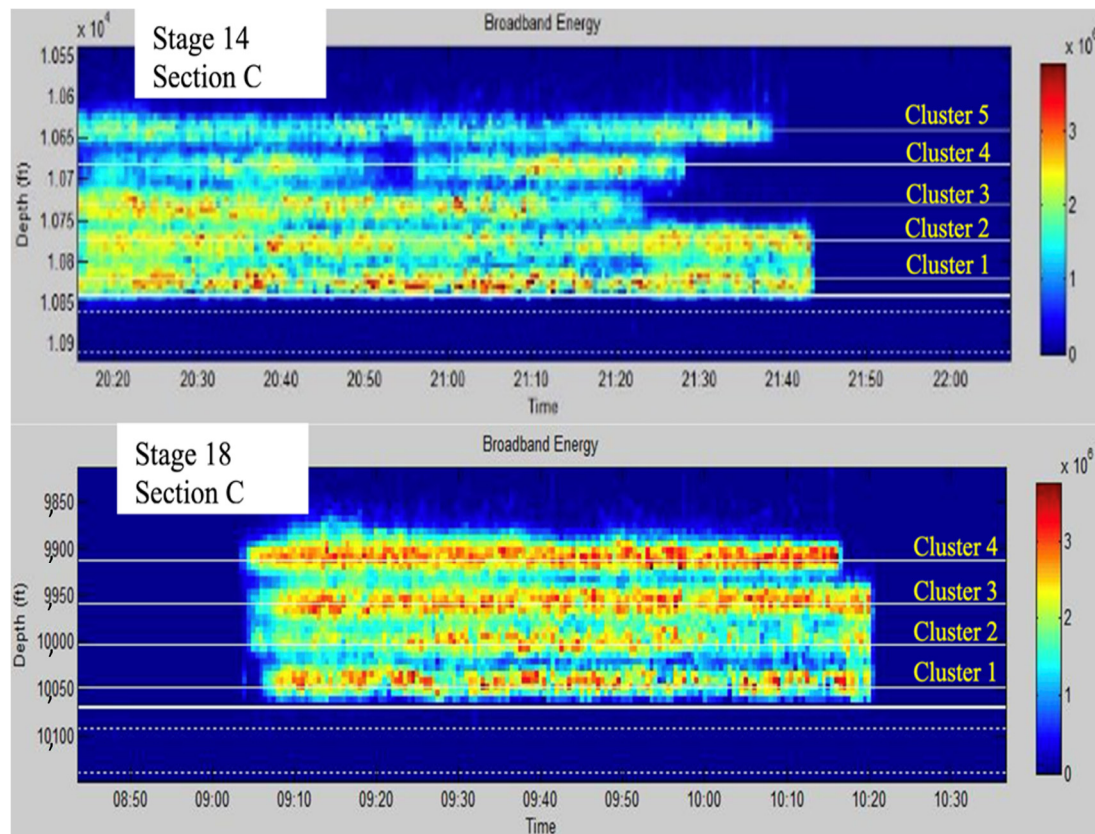

Figure 7. Broadband energy received during the fracking of section C of MIP3H, where an engineered/geomechanical completion design was used. The top shows stage 14, and the bottom shows stage 18 where a significant positive trend in DAS data response was observed in comparison to stages A and B. Both stages demonstrate an initial breakdown with good energy, indicating that there was a more synchronized and efficient initiation of fractures across all clusters, thus laying the foundation for a more balanced and effective fracture network (MIP3H completion www.mseel.com).

In Figure 8, the DTS data illustrates the initial flowback period, presenting time on the *y*-axis and the stage number on the *x*-axis for MIP 3H. The temperature was color-coded between 150 to 155 degrees Fahrenheit and averaged over 1 h. Notably, the DTS data highlights a higher production rate, as indicated by cooling, and the temperature dropped during the flowback period in section B compared with section A, except in stage 1. This observation aligns with the findings discussed earlier in Figure 6 using DAS data. The consistent higher production rate reinforced the significance of employing a shorter stage length and a greater proportion of 100 mesh sand, contributing to improved completion design efficiency and overall production in Marcellus shale. In the engineered completion design of section C, encompassing stages 13–19, the initial temperature registered lower than both sections A and B, as well as subsequent stages 20 and 21. This suggests that these sections saw enhanced production. Upon correlating the data with the design, it became evident that stages 20 and 21 (which used the experimental chemical design by Schlumberger, created using Sapphire VF) failed to yield the anticipated efficiency improvements. Interestingly, the DTS data identified stages 16, 17, 18, and 19 as the

most favorable, aside from stage 1, all of which were designed using an engineered or geomechanical approach. This emphasizes the effectiveness of such design strategies in achieving optimal production outcomes.
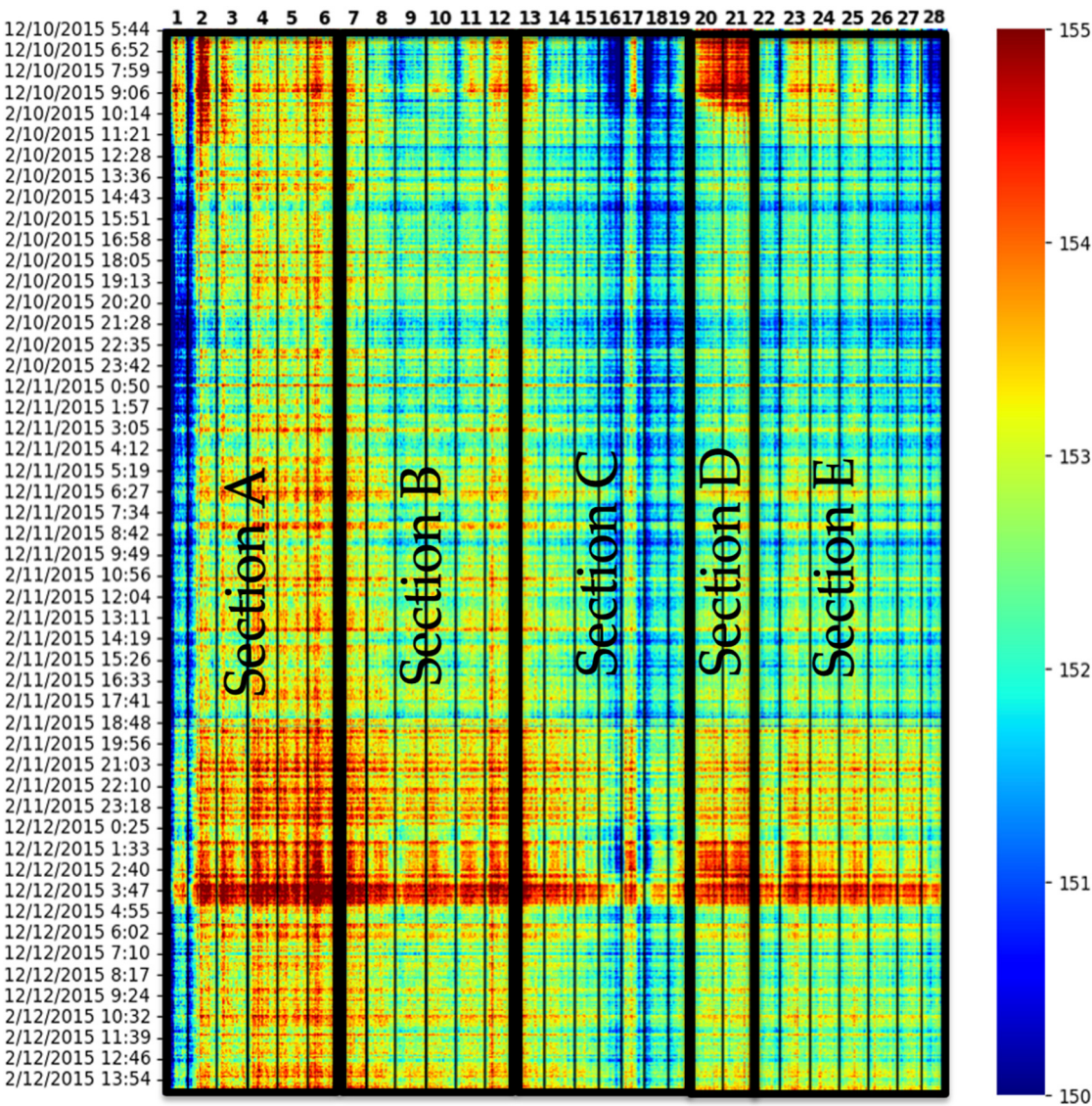

Figure 8. DTS data for the initial flow back of MIP3H, showing the contribution of different stages to production; cooler stages show higher production.

The analysis of the Production Flow Scan Imager (FSI) log, conducted on 2 March 2017, provided a comprehensive understanding of the distinct contributions of each cluster and stage to the overall gas production. Employing the Mini-Spinner Cartridge, the FSI tool measures fluid velocity and converts this information into volumetric flow rates, creating a detailed profile across the vertical cross-section of the horizontal well. In our evaluation, we computed the production contribution per lateral length for each section, and the results are presented in Table 4. Notably, Section C, distinguished by its engineered/geomechanical completion design, stands out as the primary contributor to the total production of MIP 3H, even after the extensive production period which exceeded 2 years. This finding reinforces our earlier observations derived from the completion stages of MIP3H, particularly the DAS data obtained during the stimulation period, and the DTS data obtained during the flowback period. The persistent performance of stages with a refined engineering completion design highlights their sustained impact on production, even in the later phases

of the production process. This consistent behavior aligns with the findings reported by Mahue et al. in 2022 [30], which show that initially, highly productive stages demonstrate prolonged productivity over time.

Table 4. Flow Scanner Log production analysis, 3 February 2017.

Section	Lateral Length (ft)	Production (MSCF/Day)	Production/LL (MSCF/Day/LL)
Section A	1358	1205.820	0.888
Section B	1359	1210.167	0.890
Section C	1361	1507.954	1.108
Section D	460	297.244	0.646
Section E	1518	1212.341	0.799

3.2. MSEEL Phase II (Boggess Pad)

In Phase II of the MSEEL project at the Boggess pad, Fiber Optics data serve a crucial role in a process known as far-field monitoring. This method enables the observation of reservoir responses during stimulation treatments in a monitoring well equipped with fiber optic cables, either in a similar or offset pad. Integrating near-wellbore applications (well logging) with far-field monitoring allows the generation of natural fracture network maps on both local (around the wellbore) and regional (well pad) scales. This approach proves instrumental in mitigating the impacts of well interference on the optimization of completion design.

To specifically address this objective, we gathered DSS data from both Boggess 1H and Boggess 5H wells. The DSS data were then used to quantify the magnitude of fracture driven interactions (FDI's) where the FDI is identified. As the hydraulic fracturing stimulation progressed on the treatment well, deformations emerged, which, if extended to the monitoring well equipped with fiber optics, were noted as rock tensions or compressions. This dataset can then be represented as a heatmap that depicts the magnitude of the interface between the stimulation and monitoring well.

For this specific purpose, DSS data were collected in Boggess 1H and 5H. Quantifying the magnitude of fracture-driven interactions (FDIs) between a treatment well and a monitoring well involves leveraging the values obtained from DSS data, where the FDI is identified. As the hydraulic fracturing stimulation developed on the treatment well, and fractures propagated towards the monitoring well, the DSS data were continuously collected along the fiber optic cable. This data can be visualized as a heatmap incorporating three axes, as follows: time of data collection on the *Y*-axis, measured depth of the monitoring well on the *X*-axis, and color values of pixels reflecting the intensity of the interaction on the monitoring well. In this representation, red pixels signify a rock under tension, whereas blue pixels denote a rock undergoing compression. Strong FDIs manifest as a distinct pattern on the heatmap, featuring a region of notable tension surrounded by compression, as exemplified in Figure 9.

Accompanying the DSS data, microseismic data were concurrently gathered during the hydraulic fracturing of the wells. The FDIs identified through the DSS analysis were cross-referenced with microseismic data, and a natural fracture count log was derived from Formation Microimager (FMI) logs. This cross-checking ensured that the recorded interactions were exclusively attributable to fracture driven interactions (FDI's). The location and time of FDI's were precisely located in the monitoring well and correlated with the natural fracture count values at those specific depths. This integrated approach provided a comprehensive understanding of the intricate dynamics governing hydraulic fracturing interactions, and their correlation with natural fracture networks.
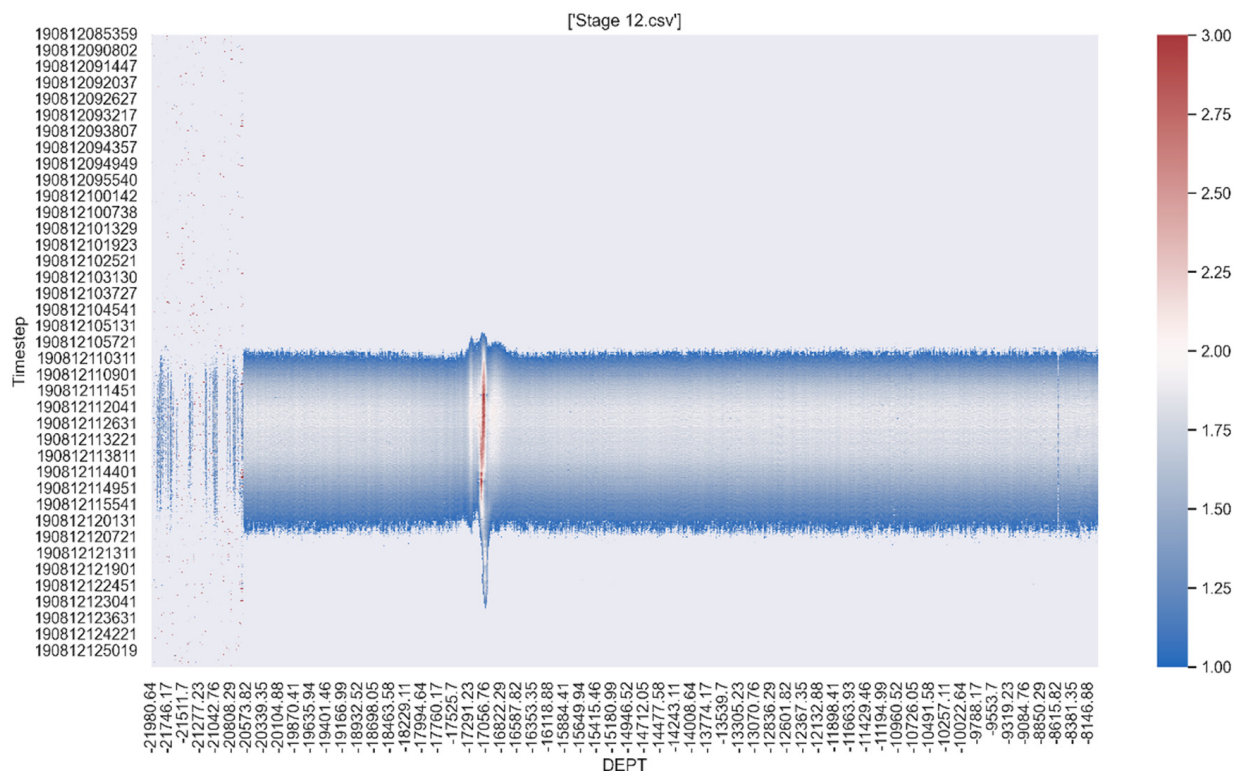
Figure 9. DSS recording indicates the frac hit on Boggess 1H during the hydraulic fracturing of Boggess 5H, stage 12.

A significant number of fracture-driven interactions (FDIs) were located in Boggess 5H while fracing the Boggess 9H (Figure 10A). These events further investigated by correlating the events with microseismic data, natural fracture counts, and distributions obtained from the formation image log (FMI). Subsequently, a Fracture-Driven Interactions (FDI) map was created to visually present the fracture-driven communication between two wells (depicted by red lines in Figure 10). The significant number of FDIs can be attributed to the short well spacing of 750 ft between these two adjacent wells in the Boggess pad. Some stimulated stages exhibited multiple interactions, a phenomenon related to the significant number of fracture counts around Boggess 5H. The majority of FDIs are in line with the direction of maximum horizontal stress, deviating only when close to intensely fractured regions. Instances with more than one fracture interaction are observed in areas with higher-than-normal fracture count values in the corresponding area of Boggess 5H, as illustrated in Figure 10A, which includes a fracture counts log along Boggess 5H.

Figure 10B depicts effective FDIs between the treatment well, Boggess 5H, and the monitoring well, Boggess 1H, with the majority of FDIs concentrated at the toe of Boggess 1H. However, both counts, and the severity of these FDIs, are reduced in comparison to those in Figure 10A, mainly due to the longer distance between Boggess 5H and Boggess 1H wells (i.e., 1500 ft). Figure 10C further demonstrates frac hits observed on Boggess 1H during the stimulation of Boggess 9H, highlighting that FDIs were observed across approximately 2250 ft of well spacing between Boggess 9H and Boggess 1H.
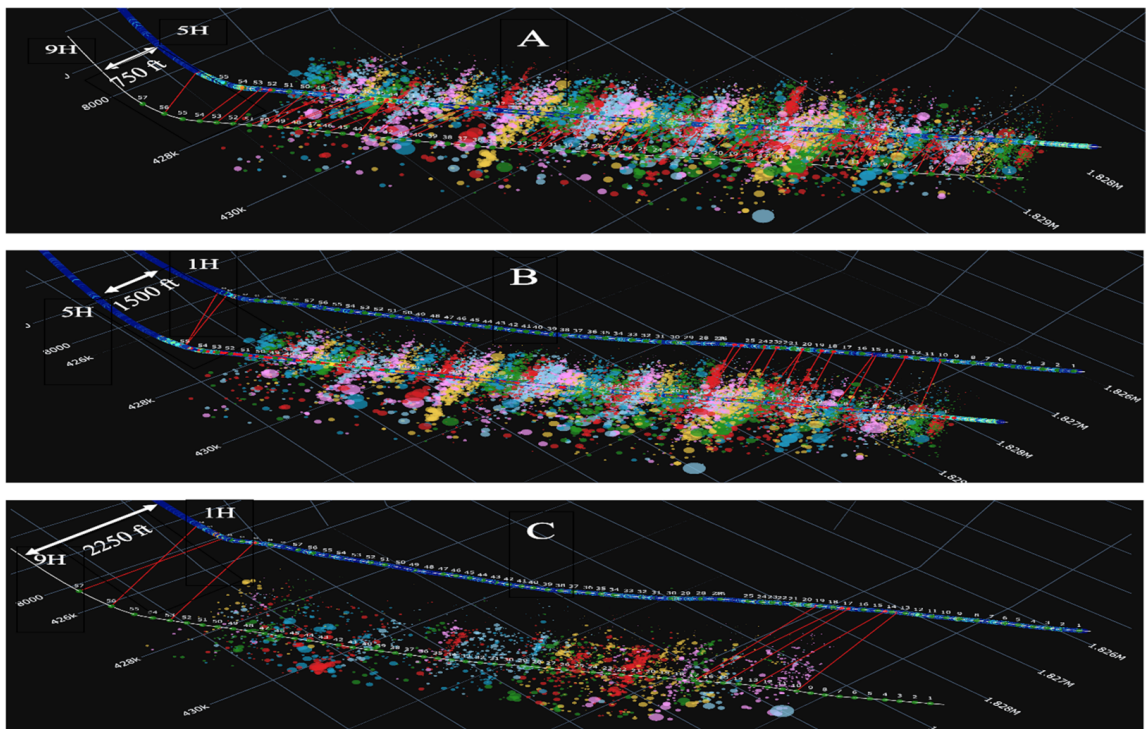
Figure 10. Fracture communications between Boggess 9H on 5H (**A**), 5H on 1H (**B**), and 9H on 1H (**C**).

In Figure 11, the distribution of normalized frac hits between Boggess 9H and Boggess 1H, Boggess 5H and Boggess 1H, and Boggess 9H and Boggess 5H is presented. As anticipated, a significant number of FDI counts with the highest intensity occurred on Boggess 5H while Boggess 9H was being fracked; this was due to the well spacings of approximately 750 ft. Fewer FDIs were observed on Boggess 1H during the stimulation of Boggess 5H. Finally, the smallest number of FDIs, with a lower intensity, was observed on Boggess 1H during the stimulation of Boggess 9H.
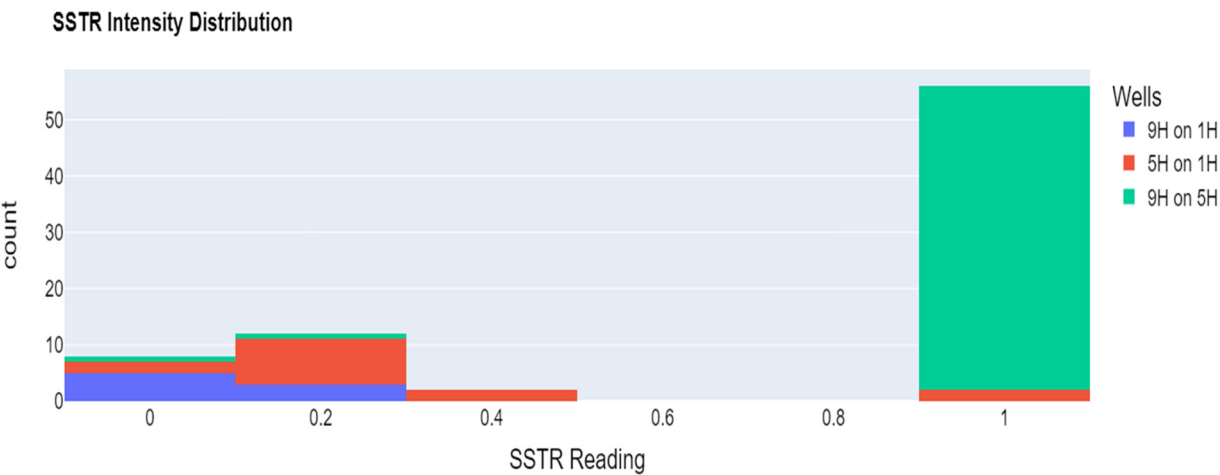

Figure 11. Frac hit normalized magnitude distribution showing the highest magnitude frac hit seen by Boggess 5H during the stimulation of 9H (i.e., 9H on 5H).

Tables A1–A3 provide detailed insights into the FDIs, as discussed in Figure 10 (Appendix A).

In Figure 12, a comprehensive 3D representation of the Boggess pad, is shown along with microseismic activities collected during the hydraulic fracturing of these wells. Gamma ray logs on Boggess 1H and 17H wells, represented by green dots, reveal plug locations, whereas red lines indicate FDIs between the wells extracted from fiber optics DSS data. The rose diagram shows the number of fractures and their orientation in Boggess 5H.
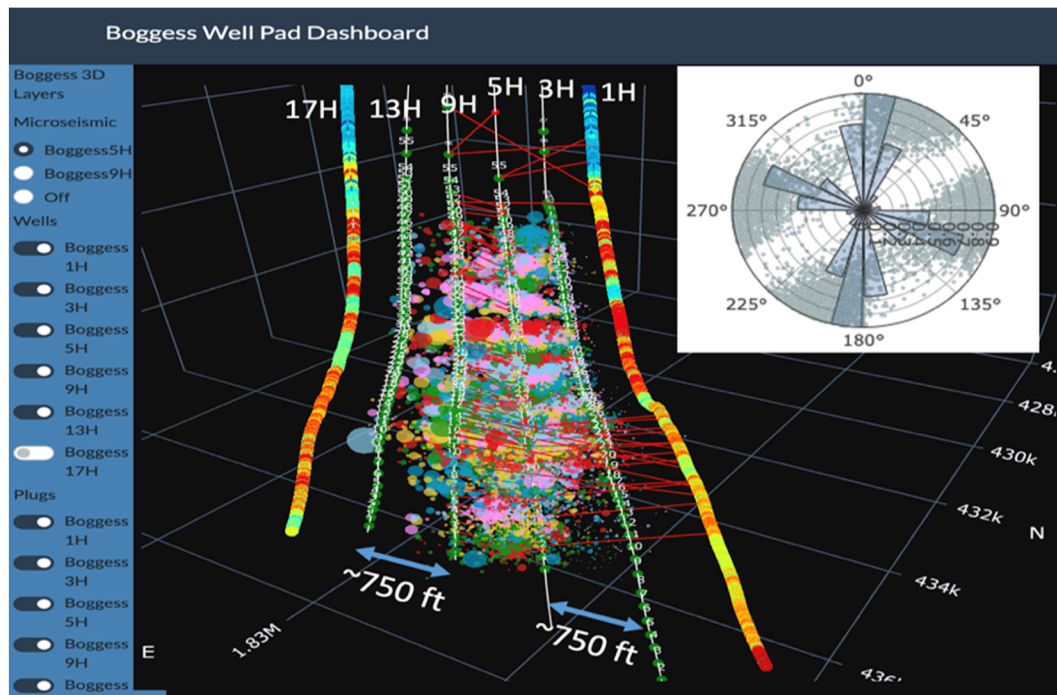

Figure 12. Three-dimensional illustration of FDIs in the Boggess Well Pad by Dr. Brian Panetta.

In Figure 13, a detailed investigation into frac communication was obtained while stimulating stage 20 in Boggess 9H. During the hydraulic fracturing of this stage, a high number of FDIs were observed in Boggess 5H stage 14 and 20. Figure 13 (Left) presents the frac hits observed on Boggess 5H during the fracking of Boggess 9H during stage 20, aligning with microseismic events and highly fractured zones. To validate the authenticity of the interaction and to eliminate potential artifacts, Figure 13 (Right) displays microseismic events observed during the fracking of Boggess 5H in stage 14. These activities align with the orientation of maximum horizontal stress, shown with a dashed blue arrow. Additionally, the seismic events also show the interaction between Boggess 5H during stage 14 and Boggess 9H during stage 20. Note that this observation occurs when stage 20 of Boggess 9H has not yet been stimulated, thus confirming a genuine communication between the wells. After integrating all the geological information, including the logs obtained while drilling, as well as micorseismic and fiberoptics data, an interactive 3D geological model that can be used for further analysis and the investigation of the completion design operations in this field was developed [31,32]. The dashboard is accessible on www.MSEEL.org and http://boggessdashboard.herokuapp.com, and provides a publicly available platform for in-depth review and study of Boggess Pad in Marcellus Shale.
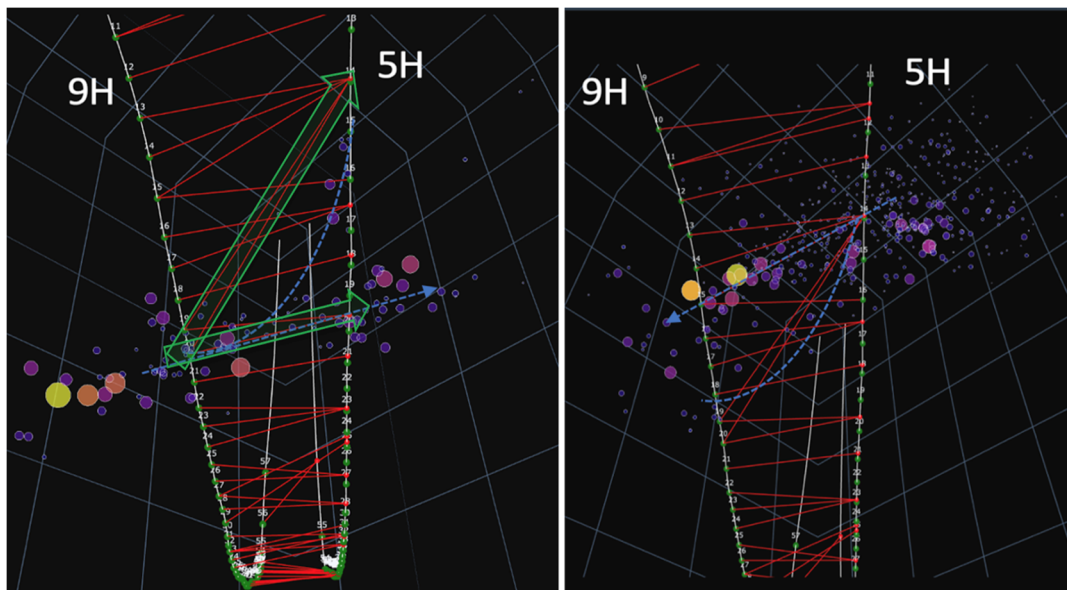
Figure 13. (**Left**): FDIs identified during stages 14 and 20 of Boggess 5H, during fracing stage 20 of Boggess 9H and 6. (**Right**): microseismic events occurred during fracing stage 14 of Boggess 5H; they were identified during stages 15 and 20 of Boggess 9H.

4. Discussions

A noteworthy limitation of our study lies in its reliance on FMI image log interpretation. We observed significant discrepancies between fracture characteristics when comparing Rose and stereonet plots generated by different consultants using the same FMI log from the Boggess 5H well. This underscores the necessity for Supplementary Data sources to validate fracture count logs or the exploration of automated workflows to mitigate the reliance on expert fracture picking from FMI logs. Addressing this limitation can serve as a compelling motivation for future research and development efforts, emphasizing the importance of refining methodologies for more robust and consistent fracture analysis in subsurface reservoirs.

5. Conclusions

In conclusion, the MSEEL projects, spanning phases I and II, which particularly focus on the MIP and Boggess pad, have underscored the critical role of an engineered/geomechanical completion design in enhancing cluster efficiency, compared with geometric or fluid mix approaches. Notably, within the MIP pad, the incorporation of a shorter stage length (SSL) and a higher concentration of 100 mesh sand enable improvements in both cluster efficiency and stage production. In a prior study [33], an analysis of the Marcellus Shale reservoir was conducted, involving an examination of over 1500 wells to ascertain the most effective well spacing and completion design parameters. This investigation utilized machine learning applications to optimize both the field-wide strategy and individual well specifications. The findings indicate that adopting a shorter stage length (SSL) and a higher sand-to-water ratio (SWR) is advantageous for Marcellus Shale, potentially leading to an enhancement of up to 8% in cumulative gas production. The positive impact of the engineered completion design is evident not only in improved cluster efficiency, as demonstrated in the MIP pad, but also in enhanced production, as corroborated by production logs. An intriguing avenue for further exploration is the correlation between natural fracture counts and cluster efficiency, as suggested by observations from MSEEL Phase I. Stages exhibiting uniform fracture density showcased superior cluster efficiency, thus influencing the subsequent completion design for the Boggess wells. The invaluable insights gained through the utilization of DAS and DTS data have revealed crucial aspects of well communication, exemplified by the frac hits observed in Boggess pad. These

findings emphasize the significance of real-time data in comprehending and optimizing stimulation processes.

Data Availability Statement: Raw data from the MIP pad and Boggess pad, including DAS, DTS, microseismic, and production logs, is available for review and analysis. The datasets are accessible to the public through the official MSEEL project website http://mseel.org/data/Wells_Datasets/. A comprehensive dashboard visualizing key findings, such as well communication, natural fracture counts, and fracture-driven interactions (FDIs), is openly accessible for review. The interactive dashboard, developed using Python and Plotly Dash, can be explored at Boggess Dashboard (http://boggessdashboard.herokuapp.com/) and MIP dashboard at (https://mipdashboard.herokuapp.com/).

Conflicts of Interest: The authors declare no conflict of interest.

Appendix A

Appendix A offers comprehensive insights into cross-well communications among Boggess 9H, 5H, and 1H, presented through detailed data in Tables A1–A3. These tables elucidate the stages exhibiting communication on the treatment well, coupled with corresponding frac hit depths on the monitoring well. The information, including scaled Steady-State Thermo Reflectance (SSTR) values, contributes to a nuanced understanding of fracture extensions in the hydraulic fracturing process.

Table A1. Boggess 5H on 1H frac hits.

5H Stage (Completion Well)	Depth on 1H (Monitoring Well)	Scaled SSTR Value
3	18,812	0.03
6	18,294	0.11
8	17,868	0.07
9	17,830	0.25
11	17,249	0.24
12	17,075	0.23
13	16,798	0.96
14	16,798	0.18
15	16,420	0.33
16	16,250	0.99
18	15,905	0.13
18	15,797	0.11
55	8225	0.27
56	8149	0.40

Table A2. Boggess 9H on Boggess 1H frac hits.

9H Stage (Completion Well)	Depth on 1H (Monitoring Well)	Scaled SSTR Value
10	18,142	0.08
13	17,966	0.02
15	17,359	0.07
17	17,000	0.13
17	17,458	0.05
53	8762	0.05
56	8170	0.10
57	8354	0.10

Table A3. Boggess 9H on Boggess 5H frac hits.

9H Stage (Completion Well)	Depth on 5H (Monitoring Well)	Scaled SSTR Value	9H Stage (Completion Well)	Depth on 5H (Monitoring Well)	Scaled SSTR Value
2	19,021	1	25	14,283	1
3	19,021	1	26	14,283	1
4	18,683	1	27	13,945	1
5	18,510	1	27	14,725	1
6	18,395	1	28	13,945	1
7	18,042	1	29	14,660	1
8	18,042	1	30	13,350	1
9	17,685	1	32	13,070	1
10	17,312	1	32	13,293	1
11	17,249	1	32	13,539	1
11	17,312	1	33	13,350	1
12	17,075	1	34	13,070	1
13	16,798	1	41	11,837	1
13	16,798	1	42	11,703	1
14	16,798	1	43	10,983	1
15	16,365	1	44	10,625	1
15	16,798	1	46	10,900	1
16	16,252	1	47	10,625	1
17	16,252	1	48	10,433	1
18	16,028	1	49	10,176	1
19	15,673	1	49	10,283	1
19	16,798	1	50	9550	1
20	15,673	1	50	9795	1
20	16,798	1	51	9920	1
21	15,400	1	52	9090	0.1
22	14,986	1	53	8963	0.3
23	14,986	1	54	8761	1
24	14,986	1	56	8303	1

References

1. Turner, R. Smart Wells—A Key Enabler for Oilfield Developments in Brunei. In Proceedings of the International Petroleum Technology Conference, Bangkok, Thailand, 7–9 February 2012; Paper IPTC 15329.
2. Muanenda, Y.; Oton, C.J.; di Pasquale, F. Application of Raman, and Brillouin Scattering Phenomena in Distributed Optical Fiber Sensing. *Front. Phys.* **2019**, *7*, 115. [CrossRef]
3. Rao, Y.-J.; Ran, Z.-L.; Gong, Y.; Güemes, A.; Sierra Perez, J. *An Introduction to Distributed Optical Fibre Sensors*; CRC Press: Boca Raton, FL, USA, 2017.

4. Zhang, S.; Zhu, D. Inversion of Downhole Temperature Measurements in Multistage-Fracturing Stimulation of Horizontal Wells in Unconventional Reservoirs. *SPE Prod. Oper.* **2020**, *35*, 231–244. [CrossRef]

5. Enright, R. Sleuth for Down-Hole Leaks. *Oil Gas J.* **1955**, *28*, 78–79.

6. Ramey, H. Wellbore Heat Transmission. *J. Pet. Technol.* **1962**, *14*, 427–435. [CrossRef]

7. Bohn, R.; Hull, R.; Trujillo, K.; Wygal, B.; Parsegov, S.G.; Carr, T.; Carney, B.J. Learnings from the Marcellus Shale Energy and Environmental Lab (MSEEL) Using Fiber Optic Tools and Geomechanical Modeling. In Proceedings of the SPE/AAPG/SEG Unconventional Resources Technology Conference, Virtual, 20–22 July 2020. [CrossRef]

8. Wu, Y.; Hull, R.; Tucker, A.; Rice, C.; Richter, P.; Wygal, B.; Farhadiroushan, M.; Trujillo, K.; Craig, W. Hydraulic Fracturing Diagnostics Utilizing Near and Far-Field Distributed Acoustic Sensing DAS Data Correspondences. In Proceedings of the SPE Hydraulic Fracturing Technology Conference and Exhibition, Virtual, 4–6 May 2021. [CrossRef]

9. Abukhamsin, A.Y. Inflow Profiling and Production Optimization in Smart Wells using Distributed Acoustic and Temperature Measurements. Ph.D. Thesis, Stanford University, Stanford, CA, USA, 2016.

10. Ghahfarokhi, P.K.; Carr, T.; Bhattacharya, S.; Elliott, J.; Shahkarami, A.; Keithan, M. A Fiber-Optic Assisted Multilayer Perceptron Reservoir Production Modeling: A Machine Learning Approach in Prediction of Gas Production from the Marcellus Shale. In Proceedings of the SPE/AAPG/SEG Unconventional Resources Technology Conference, Houston, TX, USA, 23–25 July 2018. [CrossRef]

11. Bohn, R.; Sergei, P. Diagnosing Fracture Stimulation Effectiveness: A Case Study of the Marcellus Shale Energy and Environmental Lab (MSEEL). In Proceedings of the SPE/AAPG/SEG Unconventional Resources Technology Conference, Virtual, 20–22 July 2020. [CrossRef]

12. Carr, T.; Mitchell, N.A.; Fathi, E.; Panetta, B.; Carney, B.J. Key Drivers for Complexity of Hydraulic Fracture Stimulation—Cemented and Bitumen-Filled Fractures Formed During Hydrocarbon Maturation of the Marcellus Shale—Key Drivers to Complexity of Hydraulic Fracture Stimulation. In Proceedings of the SPE/AAPG/SEG Unconventional Resources Technology Conference, Denver, CO, USA, 13–15 June 2023. [CrossRef]

13. Raab, T.; Reinsch, T.; Aldaz Cifuentes, S.R.; Henninges, J. Real-Time Well-Integrity Monitoring Using Fiber-Optic Distributed Acoustic Sensing. *SPE J.* **2019**, *24*, 1997–2009. [CrossRef]

14. Brower, D.V.; Prescott, C.N.; Zhang, J.; Howerter, C.; Rafferty, D. Real-Time Flow Assurance Monitoring with Non-Intrusive Fiber Optic Technology. In Proceedings of the Offshore Technology Conference, Houston, TX, USA, 2–5 May 2005. [CrossRef]

15. Tarek, S.; El Rahman, S.A.; Anwar, E.; Dilling, L.; Vidal, N. An Engineering Approach to Utilize Fiber Optics Telemetry Enabled Coiled Tubing (ACTive Technology) in Well Testing and Sandstone Matrix Stimulation—First Time in the World. In Proceedings of the SPE Europec/EAGE Annual Conference, Copenhagen, Denmark, 4–7 June 2012. [CrossRef]

16. Castro, L.; Lee, E.; Elliott, C.; Jesse, H. Lessons Learned from the First Application of Fiber-Optic Monitoring and Cemented Coiled Tubing-Enabled Multistage Fracturing Sleeves for Real-Time Monitoring of Stimulation Treatments and Post-Frac Production. In Proceedings of the SPE Annual Technical Conference and Exhibition, Dubai, United Arab Emirates, 26–28 September 2016. [CrossRef]

17. Fathi, E.; Adenan, M.F.; Moryan, N.; Belyadi, F.; Belyadi, H. High-Precision Single-Leak Detection and Localization in Single-Phase Liquid Pipelines Using the Negative Pressure Wave Technique: An Application in a Real-Field Case Study. *SPE J.* **2023**, *29*, 399–412. [CrossRef]

18. Martyushev, D.A.; Ponomareva, I.N.; Filippov, E.V. Studying the direction of hydraulic fracture in carbonate reservoirs: Using machine learning to determine reservoir pressure. *Pet. Res.* **2023**, *8*, 226–233. [CrossRef]

19. Gao, Q.; Cheng, Y.; Fathi, E.; Ameri, S. Analysis of stress-field variations expected on subsurface faults and discontinuities in the vicinity of hydraulic fracturing. *SPE Reserv. Eval. Eng.* **2016**, *19*, 54–69. [CrossRef]

20. Van Thang, N.; Thang Vinh, P.; Rogachev, M.; Korobov, G.; Zhurkevich, A.; Islamov, S. A comprehensive method for determining the dewaxing interval period in gas lift wells. *J. Pet. Explor. Prod. Technol.* **2023**, *13*, 1163–1179. [CrossRef]

21. Johannessen, K.; Drakeley, B.; Farhadiroushan, M. Distributed Acoustic Sensing—A New Way of Listening to Your Well/Reservoir. In Proceedings of the Intelligent Energy International Conference and Exhibition, Utrecht, The Netherlands, 27–29 March 2012. Paper SPE 149602.

22. Paleja, R.; Mustafina, D.; In't Panhuis, P.; Park, T.; Randell, D.; van der Horst, J.; Crickmore, R. Velocity Tracking for Flow Monitoring and Production Profiling Using Distributed Acoustic Sensing. In Proceedings of the Annual Technical Conference and Exhibition, Houston, TX, USA, 28–30 September 2015. Paper SPE 174823.

23. Wang, Z. The Uses of Distributed Temperature Survey (DTS) Data. Ph.D. Thesis, Department of Energy Resources Engineering, Stanford University, Stanford, CA, USA, 2012.

24. Fathi, E.; Carr, T.; Adenan, M.F.; Panetta, B.; Kumar, A.; Carney, B.J. High-quality fracture network mapping using high frequency logging while drilling (LWD) data: MSEEL case study. *Mach. Learn. Appl.* **2022**, *10*, 100421. [CrossRef]

25. Carr, T.; Fathi, E.; Bohn, R.; Adenan, M.F.; Li, L.; Panetta, B.; Carney, B.J.; Mitchell, N. Importance of Preexisting Fractures to Completion and Production Efficiencies in the Marcellus Shale Energy and Environmental Lab MSEEL. In Proceedings of the SPE Hydraulic Fracturing Technology Conference and Exhibition, The Woodlands, TX, USA, 1–3 February 2022. [CrossRef]

26. Carr, T.; Ghahfarokhi, P.K.; Carney, B.J.; Hewitt, J.; Vargnetti, R. Marcellus Shale Energy and Environmental Laboratory (MSEEL) Results and Plans: Improved Subsurface Reservoir Characterization and Engineered Completions. In Proceedings of the Unconventional Resources Technology Conference, Denver, CO, USA, 22–24 July 2019. [CrossRef]

27. Belyadi, H.; Fathi, E.; Belyadi, F. *Hydraulic Fracturing in Unconventional Reservoirs: Theories, Operations, and Economic Analysis*, 2nd ed.; Gulf Professional Publishing: Houston, TX, USA, 2019.

28. Hull, R.; Woerpel, C.; Trujillo, K.; Bohn, R.; Wygal, B.; Carney, B.J.; Carr, T. Hydraulic fracture characterization using fiber optic DAS and DTS data. In Proceedings of the SEG International Exposition and Annual Meeting, Virtual, 11–16 October 2020. [CrossRef]

29. Pham, V.; Fathi, E.; Belyadi, F. New Hybrid Approach for Developing Automated Machine Learning Workflows: A Real Case Application in Evaluation of Marcellus Shale Gas Production. *Fuels* **2021**, *2*, 286–303. [CrossRef]

30. Mahue, V.; Jimenez, E.; Dawson, P.; Trujillo, K.; Robert, H. Repeat DAS and DTS Production Logs on a Permanent Fiber Optic Cable for Evaluating Production Changes and Interference with Offset Wells. In Proceedings of the SPE/AAPG/SEG Unconventional Resources Technology Conference, Houston, TX, USA, 20–22 June 2022. [CrossRef]

31. Panetta, B.; Carr, T.; Fathi, E. 3D visualization of integrated geologic and geophysical subsurface data using open-source programming: A case study using data from the MSEEL project. In *Second International Meeting for Applied Geoscience & Energy*; Society of Exploration Geophysicists and American Association of Petroleum Geologists: Tulsa, OK, USA, 2022; pp. 3508–3512.

32. Panetta, B.; Carr, T.; Fathi, E. Interactive 3D Visualization of Integrated Geologic and Geophysical Subsurface Data Using Python. *CONNECTS* **2023**, *55*, 3508–3512. [CrossRef]

33. Fathi, E.; Takbiri-Borujeni, A.; Belyadi, F.; Adenan, M.F. Simultaneous Well Spacing and Completion Optimization Using Automated Machine Learning Approach. A Case Study of Marcellus Shale Reservoir in the North-Eastern United States. *Pet. Geosci.* **2024**, petgeo2023-077R1. [CrossRef]